Supplementary materials

The nexus between urbanization and precipitation chemistry in the Pearl River Delta, China: Decoupling analysis

Na Wang[1], Le Li[2], Xinfeng Zhao[3,4], Yingxue Xuan[5], Zebin Zhang[3,4], Hong Yang[3,4], Lingling Zhao[1,*]

[1] Guangdong Provincial Observation and Research Station for Urban Agglomeration Ecosystem in Guang-dong-Hong Kong-Macao Greater Bay Area, Guangzhou Institute of Geography, Guangdong Academy of Sciences, Guangzhou 510070, China; wangn929@163.com / wangnll821@gdas.ac.cn (N.W.)

[2] Research Institute of Tropical Forestry, Chinese Academy of Forestry, Guangzhou 510520, China; zglkylile@163.com / ritflile@caf.ac.cn (L.L.)

[3] Zhuhai Ecological Environment Monitoring Station of Guangdong Province, Zhuhai 519070, China; xin-fengzhao@foxmail.com (X.Z.); zd8016@163.com (Z.Z.); michelleyang05@163.com (H.Y.)

[4] Guangdong Pearl River Estuary Integrated Monitoring Station for Ecological Quality of Marine Ecosystem, Zhuhai 519070, China

[5] Guangdong Provincial Key Laboratory of Applied Botany, Key Laboratory of National Forestry and Grassland Administration on Plant Conservation and Utilization in Southern China, South China Bo-tanical Garden, Chinese Academy of Sciences, Guangzhou, 510650, China; xuanyx@scbg.ac.cn (Y.X.)

***Corresponding author**: Prof. Lingling Zhao

E-mail: linglingzhao@foxmail.com (L.Z.); Tel: 020-87685006

Address: No. 100, Xian-Lie Middle Road, Yuexiu District, Guangzhou 510070, China

1 Supplementary Tables

Table S1. Basic information of the 29 precipitation monitoring sites in the PRD.

City	Site name	Site No	Classification	Latitude	Longitude	Samples
Guangzhou	Yuexiu	1	Urban	23.13	113.26	1826
	Baiyun	2	Urban	23.18	113.30	1612
	Huangpu	3	Urban	23.11	113.44	1411
	Panyu	4	Urban	22.94	113.35	1288
Shenzhen	Meiao	5	Urban	22.55	114.10	1907
	Luohu	6	Urban	22.58	114.13	1299
	Futian	7	Urban	22.55	114.06	1450
	Nanshan	8	Urban	22.50	113.91	1615
	Yantian	9	Urban	22.55	114.23	1328
	Baoan	10	Urban	22.57	113.91	1262
	Longgang	11	Urban	22.72	114.26	1058
	Yangmeikeng	12	Suburb	22.54	114.59	643
Zhuhai	Xiangzhou	13	Urban	22.27	113.57	1492
Foshan	Chancheng	14	Urban	23.01	113.08	1860
	Nanhai	15	Urban	23.03	113.14	1166
	Shunde	16	Urban	22.85	113.23	1077
	Gaoming	17	Urban	22.89	112.87	1350
	Sanshui	18	Urban	23.17	112.89	1365
Jiangmen	Pengjiang	19	Urban	22.58	113.07	1321
	Jianghai	20	Urban	22.58	113.09	1293
	Tangxia	21	Suburb	22.68	113.03	1168
	Xinhui	22	Urban	22.53	113.04	1383
Zhaoqing	Duanzhou	23	Urban	23.05	112.47	1629
Huizhou	Huicheng	24	Urban	23.07	114.41	1630
	Aibei	25	Suburb	23.23	114.65	1029
Dongguan	Dongcheng	26	Urban	23.05	113.76	1853
	Guancheng	27	Urban	23.04	113.74	1747
Zhongshan	Shiqi	28	Urban	22.52	113.37	1530
	Huoju	29	Suburb	22.49	113.43	1409

Table S2. Semivariogram parameters of nighttime light index at different extent levels.

Extent (km)	Nugget	Sill	Nugget/ Sill	Range	RSS	R^2	Model
1	1.379	3.445	0.400	123800	0.213	0.921	Spherical
2	0.914	2.521	0.363	118700	0.177	0.949	Spherical
3	0.604	1.914	0.316	114400	0.178	0.953	Spherical
4	0.485	1.632	0.297	112800	0.137	0.962	Spherical
5	0.330	1.452	0.227	115700	0.111	0.974	Spherical
6	0.218	1.160	0.188	115200	0.086	0.986	Spherical
7	0.144	0.982	0.147	114600	0.093	0.985	Spherical
8	0.139	0.951	0.146	112400	0.102	0.979	Spherical
9	0.074	0.713	0.104	117000	0.127	0.978	Spherical
10	0.014	0.605	0.023	126800	0.158	0.973	Spherical

Table S3. Semivariogram parameters of population density index at different extent levels.

Extent (km)	Nugget	Sill	Nugget/ Sill	Range	RSS	R^2	Model
1	1.300	3.896	0.334	112500	0.565	0.936	Spherical
2	1.153	3.813	0.302	114000	0.531	0.943	Spherical
3	1.051	3.687	0.285	116400	0.481	0.947	Spherical
4	1.020	3.640	0.280	115900	0.497	0.954	Spherical
5	0.927	3.674	0.252	116500	0.545	0.966	Spherical
6	0.925	3.643	0.254	114800	0.460	0.971	Spherical
7	0.851	3.619	0.235	112800	0.473	0.968	Spherical
8	1.000	3.597	0.278	108400	0.499	0.968	Spherical
9	0.724	3.548	0.204	118300	0.565	0.967	Spherical
10	1.133	3.790	0.299	118700	0.548	0.966	Spherical

Table S4. Semivariogram parameters of construction land proportion index at different extent levels.

Extent (km)	Nugget	Sill	Nugget/ Sill	Range	RSS	R^2	Model
1	1.292	2.866	0.451	91300	1.04	0.713	Spherical
2	1.061	2.920	0.363	102900	0.721	0.847	Spherical
3	0.844	2.899	0.291	109700	0.484	0.923	Spherical
4	0.652	2.827	0.231	115200	0.374	0.950	Spherical
5	0.514	2.779	0.185	118500	0.307	0.975	Spherical
6	0.403	2.748	0.147	122400	0.223	0.989	Spherical
7	0.324	2.735	0.118	124600	0.299	0.985	Spherical
8	0.268	2.677	0.100	125500	0.374	0.986	Spherical
9	0.233	2.675	0.087	126800	0.478	0.979	Spherical
10	0.176	2.609	0.067	128400	0.354	0.981	Spherical

Table S5. The precipitation ion concentration in the PRD from 2000 to 2020 (μeq L^{-1}).

Year	SO_4^{2-}	NO_3^-	Cl^-	F^-	Ca^{2+}	NH_4^+	Na^+	K^+	Mg^{2+}
2000	103.21±55.15	28.48±13.16	27.44±10.86	12.45±6.45	62.28±33.46	44.63±16.74	20.34±9.95	9.24±5.2	7.45±2.85
2001	123.45±55.29	36.68±16.33	36.49±19.24	15.51±5.19	64.03±31.79	48.81±18.01	15.94±7.14	6.85±2.81	6.74±1.88
2002	135.71±32.35	36.62±9.88	52.13±21.79	12.66±3.23	66.83±27.9	73.61±17.2	23.45±6.95	18.83±13.8	9.79±4.56
2003	153.15±48.66	52.38±14.79	44.03±12.28	22.3±10.2	90.51±26.18	76.01±16.83	52.7±32.87	12.52±5.81	11.19±1.86
2004	202.58±78.52	53.61±19.8	46.77±16.1	16.95±10.51	132.23±54.81	63.98±12.32	34.96±20.54	9.84±7.01	11.39±4.44
2005	176.84±63.15	55.19±31.8	52.22±18.7	18.79±8.63	154.64±81.98	68.76±14.65	74.87±52.6	13.81±5.98	16.36±7.95
2006	171.54±66.19	50.74±18.93	48.59±16.72	15.27±7.61	133.48±53.72	58.37±8.67	53.47±48.08	13.82±6.62	17.39±8.01
2007	131.75±55.37	37.28±14.97	37.03±15.77	13.34±7.92	110.51±85.22	59.26±29.14	21.39±18.83	10.35±9.66	10.63±7.72
2008	115.84±38.66	35.72±11.76	46.31±20.63	11.5±6.72	82.69±36.64	50.64±12.71	31.92±22.53	19.06±17.03	11.77±7.32
2009	113.34±34.31	44.32±16.08	49.01±18.75	12.09±6.4	74.84±35.26	60.21±23.99	21.98±6.85	24.08±18.3	11.92±6.89
2010	100.67±30.15	51.7±25.4	38.38±17.04	9.92±5.58	79.83±43.47	50.13±17.1	24.81±10.46	16.09±14.62	15.93±9.4
2011	98.76±41.14	40.24±20.5	35.94±29.45	8.37±5.21	83.82±67.22	53.57±26.22	24.2±17.24	16.79±23.05	16.01±15.96
2012	77.54±36.96	33.31±14.7	26.94±24.25	6.55±5.62	41.04±35.23	47.32±30.41	15.13±15.44	10.31±13.67	11.03±10.06
2013	63.55±32.54	31.49±12.22	21.09±11.27	4.94±4.41	43.27±37.2	35.14±24.99	14.55±12.26	6.64±6.67	8.76±9.14
2014	77.66±44.55	42.69±19.34	29.31±16.96	7.9±6.13	52.44±49.48	46.61±27.08	20.73±17.24	9.99±9.79	12.54±10.66
2015	58.84±34.87	34.85±14.31	26.76±14.98	5.29±3.9	35.58±26.76	34.31±23.78	15.07±11.57	6.74±10.72	7.43±6.96
2016	53.83±30.84	32.89±13.68	27.05±21.45	4.41±3.14	31.51±29.28	33.67±21.26	13.75±9.67	7.26±8.87	6.96±5.12
2017	35.02±14.25	23.39±7.48	25.31±15.56	4.11±4.49	27.42±26.34	27.84±21.86	13.81±11.14	7.18±11.9	6.02±4.11
2018	39.41±19.72	26.38±9.89	34.95±30.71	3.25±3.11	28.81±29.1	28.16±24.65	18.57±21.17	5.49±9.05	6.95±8.02
2019	29.51±7.68	29.07±6.86	26.33±20.62	4.04±4.61	22.41±12.57	33.75±18.53	10.65±7.71	5.41±5.81	5.46±3.01
2020	33.38±28.06	30.4±11.9	25.22±15.4	4.57±7.27	28.17±19.83	35.03±19.06	13.97±11.43	5.86±8.49	6.53±6.16

Note: the data is means ± standard deviation.

Table S6. The optimal discretization method and the number of strata of the OPGD model.

Dependent variable	Independent variable	Discretization method					Number of strata				
		2000	2005	2010	2015	2020	2000	2005	2010	2015	2020
SO_4^{2-}	NTL	sd	equal	quantile	sd	sd	7	7	5	4	7
	CUI	natural	sd	quantile	natural	geometric	7	7	6	7	6
	POD	natural	geometric	geometric	geometric	geometric	5	7	7	7	7
	CLP	natural	quantile	geometric	sd	sd	7	7	7	7	7
NO_3^-	NTL	sd	geometric	natural	natural	equal	7	7	7	6	5
	CUI	natural	equal	natural	natural	equal	7	7	7	7	7
	POD	natural	equal	geometric	geometric	quantile	5	3	7	7	5
	CLP	equal	equal	natural	quantile	geometric	7	5	7	7	7
Ca^{2+}	NTL	sd	equal	quantile	sd	geometric	7	7	6	7	4
	CUI	natural	natural	geometric	sd	geometric	7	7	6	7	6
	POD	natural	quantile	geometric	geometric	quantile	5	6	7	7	7
	CLP	natural	quantile	sd	sd	sd	7	7	7	7	7
NH_4^+	NTL	sd	quantile	quantile	geometric	geometric	7	6	5	4	4
	CUI	natural	sd	quantile	sd	sd	7	7	7	7	4
	POD	sd	quantile	geometric	geometric	geometric	7	6	7	7	7
	CLP	natural	natural	geometric	quantile	equal	7	7	6	6	7

Table S7. The decoupling types and characteristics of precipitation ion concentration (PIC) and urbanization factor (UF).

DCI type	DCI value range	Subsystem characteristic	Decoupling characteristic	Subsystem type
Coupling (A)	$0.8 < DCI < 1.2$	$\%\Delta PIC > 0$ $\%\Delta UF > 0$	Expansive coupling	A1
	$0.8 < DCI < 1.2$	$\%\Delta PIC < 0$ $\%\Delta UF < 0$	Recessive coupling	A2
Decoupling (B)	$0 < DCI < 0.8$	$\%\Delta PIC > 0$ $\%\Delta UF > 0$	Weak decoupling	B1
	$DCI < 0$	$\%\Delta PIC < 0$ $\%\Delta UF > 0$	Strong decoupling	B2
	$DCI > 1.2$	$\%\Delta PIC < 0$ $\%\Delta UF < 0$	Recessive decoupling	B3
Negative decoupling (C)	$DCI > 1.2$	$\%\Delta PIC > 0$ $\%\Delta UF > 0$	Expansive negative decoupling	C1
	$DCI < 0$	$\%\Delta PIC > 0$ $\%\Delta UF < 0$	Strong negative decoupling	C2
	$0 < DCI < 0.8$	$\%\Delta PIC < 0$ $\%\Delta UF < 0$	Weak negative decoupling	C3

Table S8. Mann–Kendall trend test of interannual changes of the precipitation ion concentration in the PRD from 2000 to 2020.

Ionic component	2000–2008			2009–2020			2000–2020		
	Mean	Z	*p*	Mean	Z	*p*	Mean	Z	*p*
SO_4^{2-}	146.008	0.521	0.602	65.126	−3.909	<0.001	99.790	−4.741	<0.001
NO_3^-	42.966	0.521	0.602	35.060	−2.674	<0.01	38.448	−2.627	<0.01
Cl^-	43.445	0.938	0.348	30.523	−2.263	<0.05	36.061	−3.171	<0.01
F^-	15.420	−0.313	0.755	6.287	−3.360	<0.001	10.201	−4.801	<0.001
Ca^{2+}	99.690	1.772	0.076	45.762	−3.223	<0.01	68.874	−3.533	<0.001
NH_4^+	60.452	0	1	40.479	−2.949	<0.01	49.039	−3.835	<0.001
Na^+	36.559	1.147	0.252	17.269	−2.537	<0.05	25.536	−3.171	<0.01
K^+	12.703	1.564	0.118	10.154	−3.223	<0.01	11.247	−2.325	<0.05
Mg^{2+}	11.411	2.189	<0.05	9.628	−3.223	<0.01	10.392	−1.782	0.075

Table S9. Mann-Kendall trend test of interannual change of total ion concentration change in precipitation in the PRD from 2000 to 2020.

Ionic component	2000–2008			2009–2020			2000–2020		
	Mean	Z	*p*	Mean	Z	*p*	Mean	Z	*p*
TAC	247.839	0.521	0.602	136.997	−3.497	<0.001	184.500	−4.318	<0.001
TCC	220.815	1.355	0.175	123.292	−3.360	<0.001	165.088	−3.835	<0.001
TIC	468.654	1.147	0.252	260.289	−3.772	<0.001	349.588	−4.137	<0.001

Table S10. Global bivariate Moran's *I* between the precipitation ion concentration (PIC) and urbanization factor (UF) in the PRD from 2000 to 2020.

Type	2000	2005	2010	2015	2020
SO_4^{2-}–POD	−0.004	−0.082	0.088	−0.143	0.007
SO_4^{2-}–NTL	−0.111	−0.007	0.090	-0.181	0.186
SO_4^{2-}–CLP	−0.086	−0.023	0.092	−0.180	0.077
SO_4^{2-}–CUI	−0.099	−0.023	0.096	−0.191	0.146
NO_3^-–POD	−0.052	0.187	−0.083	−0.029	0.154
NO_3^-–NTL	−0.175	−0.053	−0.240	0.080	0.340
NO_3^-–CLP	−0.101	0.048	−0.155	−0.007	0.238
NO_3^-–CUI	−0.153	0.007	−0.206	0.044	0.317
Ca^{2+}–POD	0.021	−0.094	0.148	0.003	0.005
Ca^{2+}–NTL	−0.084	−0.041	0.134	0.076	0.192
Ca^{2+}–CLP	−0.083	−0.049	0.117	0.003	0.077
Ca^{2+}–CUI	−0.077	−0.054	0.138	0.049	0.149
NH_4^+–POD	−0.005	0.024	0.076	−0.072	−0.102
NH_4^+–NTL	−0.100	0.054	0.072	−0.185	−0.127
NH_4^+–CLP	−0.096	0.069	0.072	−0.144	−0.129
NH_4^+–CUI	−0.095	0.060	0.077	−0.173	−0.138

Table S11. The Pearson correlation coefficient between precipitation ion concentration (PIC) and urbanization factor (UF) from 2000 to 2020 in the PRD.

Year	2000	2005	2010	2015	2020
SO_4^{2-}–NTL	−0.108***	−0.009	0.097***	−0.178***	0.188***
NO_3^-–CUI	−0.153***	0.025	−0.211***	0.048	0.319***
Ca^{2+}–NTL	−0.080**	−0.042	0.138***	0.087***	0.199***
NH_4^+–NTL	−0.095***	0.052	0.081**	−0.177***	−0.121***

Note: ** and *** represent $p < 0.01$ and 0.001, respectively.

Table S12. Values of NH_4^+/NO_3^- at the 29 deposition monitoring sites in the PRD from 2000 to 2020.

City	Site name	2000–2008	2009–2020
Shenzhen	Luohu	1.637	0.578
	Futian	1.621	0.696
	Nanshan	1.411	0.763
	Yantian	1.552	0.503
	Baoan	1.428	0.686
	Longgang	1.513	0.679
	Yangmeikeng	1.427	0.873
Zhaoqing	Duanzhou	1.365	6.263

Table S13. Comparative overview of decoupling characteristics between urbanization and diverse environmental stressors across different spatial scales.

Region	Urbanization factor	Environmental stressor	Dominant decoupling trajectory	Key drivers	Ecological/environmental implications
This study (PRD)	Nighttime lights (NTL) intensity, built-up area, gridded population	Precipitation chemistry (SO_4^{2-}, NO_3^-, Ca^{2+}, NH_4^+, etc.)	expansive negative decoupling (END) (pre-2005) →strong decoupling (SD) (post-2005, up to 75.86%)	Economic urbanization, industrial restructuring, emission controls	Shift from sulfate-dominated to mixed sulfate–nitrate precipitation; reduced acid deposition risk but potential nitrogen saturation; non-stationary spatial trade-offs between core and periphery
Wu et al. (2024) / Zhejiang Province	New-Type Urbanization (NTU) index (population, economic, social, environmental dimensions)	County-level carbon emissions (CE)	Suboptimal (2007–2012) → SD-II (60.7% by 2017–2021)	Evolving from economic NTU (2007) to societal NTU (2012) and population NTU (2021)	Significant CE reduction in northern counties; persistent spatial disparity in CE intensity; green transition facilitated by low-carbon industrial policies
Zhang et al. (2026) / 19 Chinese urban agglomerations	Comprehensive urbanization (spatial, economic, population)	Multiple ecosystem services (carbon storage, water retention, soil conservation, habitat quality)	Weak decoupling (WD, 44%) and END (25%) dominant; SD (only 8–12%)	Core-periphery divide along the Bole–Taipei Line; rapid urban land expansion	Habitat quality degradation in southeastern coastal cities; manageable ecological pressure in most regions but severe ecosystem service decline in shrinking cities (e.g., Northeast China)
Sun et al. (2023) / Taihu Lake Basin	Urbanization rate	Agricultural nonpoint source pollution (total nitrogen [TN], total phosphorus [TP])	Basin-wide decoupling achieved; TN (strong decoupling) outperformed TP (WD / END)	Intensity effect & structure effect promoted SD; output effect & population effect induced END / expansive coupling (EC)	Improved water quality for TN but TP rebound risk; livestock and poultry breeding remained a concentrated source; urban–rural collaborative governance needed
Liu et al. (2025) / Yellow River Basin	Multi-dimensional urbanization (population, economic, spatial, social)	Atmospheric environment ($PM_{2.5}$, SO_2, NO_2, etc.)	Weak decoupling dominant; transient END during 2014–2017 following new air quality standards (GB 3095–2012)	Environmental policy stringency, energy structure adjustment, clean energy penetration	Air quality improvement in middle-lower reaches; persistent pressure in Shanxi (coal-industry-dominated SO_2 emissions); spatial gradient of "high coordination in middle-lower, low in upper" reaches

References

Wu, Y.Q.; Zhou, C.Y.; Lai, X.Y.; Li, Y.H.; Miao, L.T.; Yu, H.F. Spatio-temporal characteristics and decoupling relationship of new-type urbanization and carbon emissions at the county Level: A case study of Zhejiang Province, China. *Ecol. Indic.* **2024**, *160*, 111793. https://doi.org/10.1016/j.ecolind.2024.111793.

Zhang, L.F.; Fang, C.L.; Zhu, C. Coupling coordination and decoupling effects: Measuring the interaction between urban agglomeration ecosystems and urbanization. *Cities* **2026**, *171*, 106788. https://doi.org/10.1016/j.cities.2026.106788.

Sun, D.Y.; Wang, X.X.; Yu, M.L.; Ouyang, Z.L.; Liu, G. Dynamic evolution and decoupling analysis of agricultural nonpoint source pollution in Taihu Lake Basin during the urbanization process. *Environ. Impact Asses. Rev.* **2023**, *100*, 107048. https://doi.org/10.1016/j.eiar.2023.107048.

Liu, F.F.; Zhu, M.Y.; Hua, C.Y.; Wang, L.; Tian, Y.R.; Fang, S.M.; Yang, J.Y.; Ren, L.J. Spatiotemporal analysis of the coupling and decoupling relationship between urbanization and atmospheric environment in the Yellow River Basin of China. *Theor. Appl. Climatol.* **2025**, *156*, 274. https://doi.org/10.1007/s00704-025-05511-1.

2 Supplementary Figures

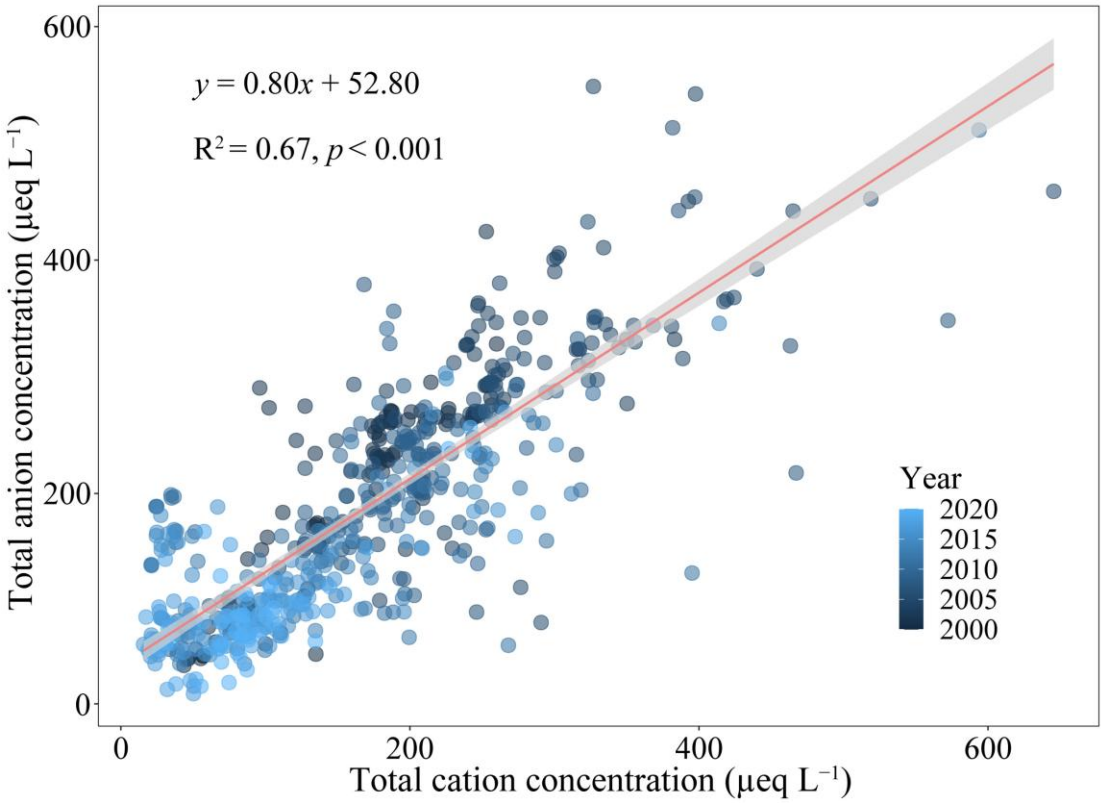


Figure S1. Linear regression fitting between anion and cation concentrations (*n* = 604).

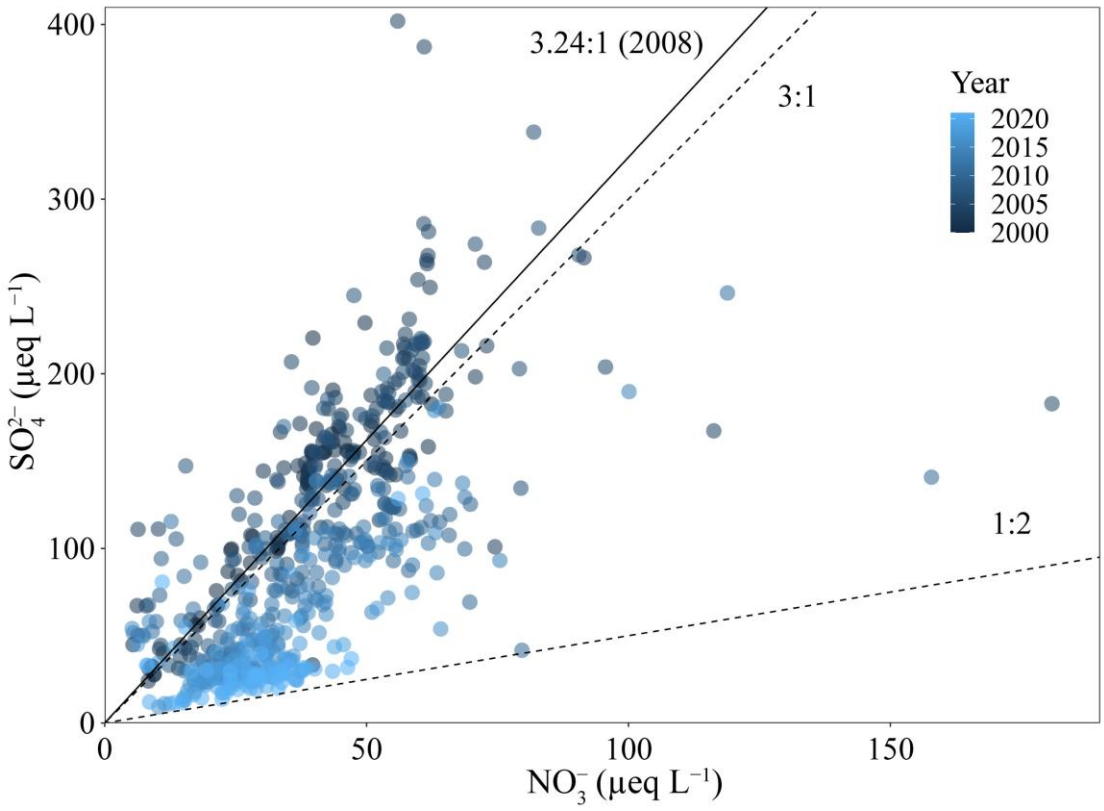


Figure S2. Characteristics of acid balance in precipitation from 2000 to 2020.

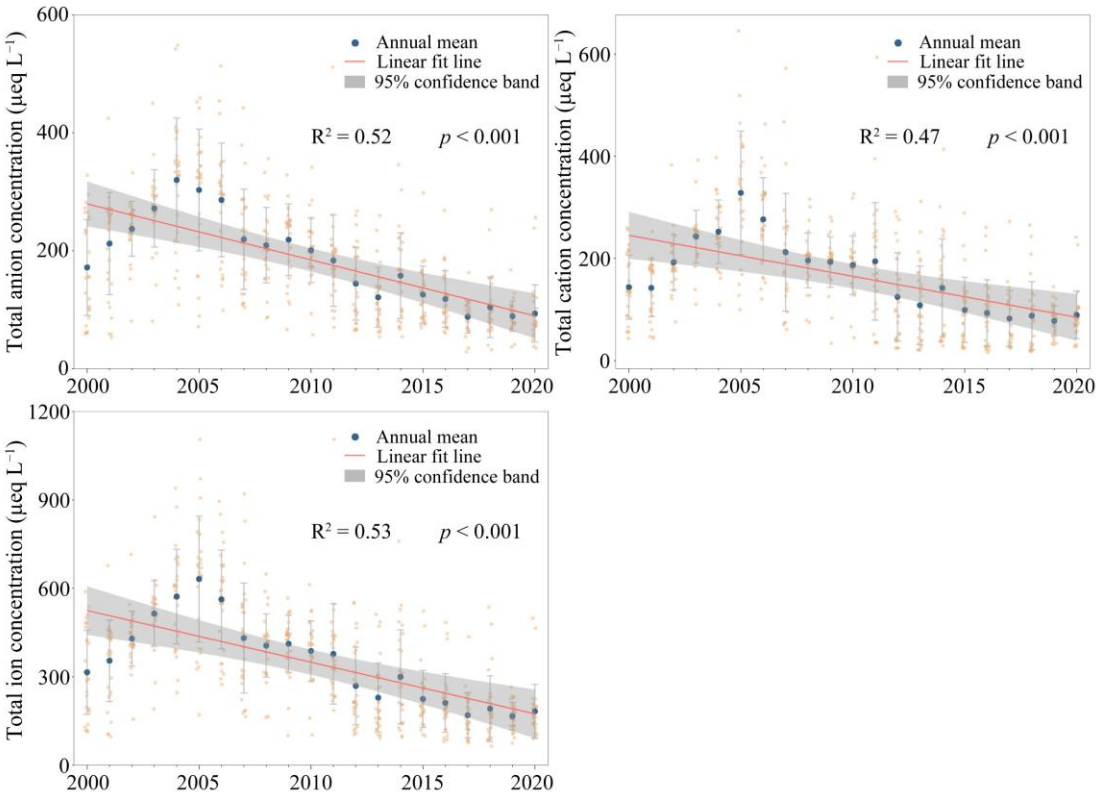


Figure S3. Temporal variation of total ion concentration in precipitation in the PRD from 2000 to 2020.

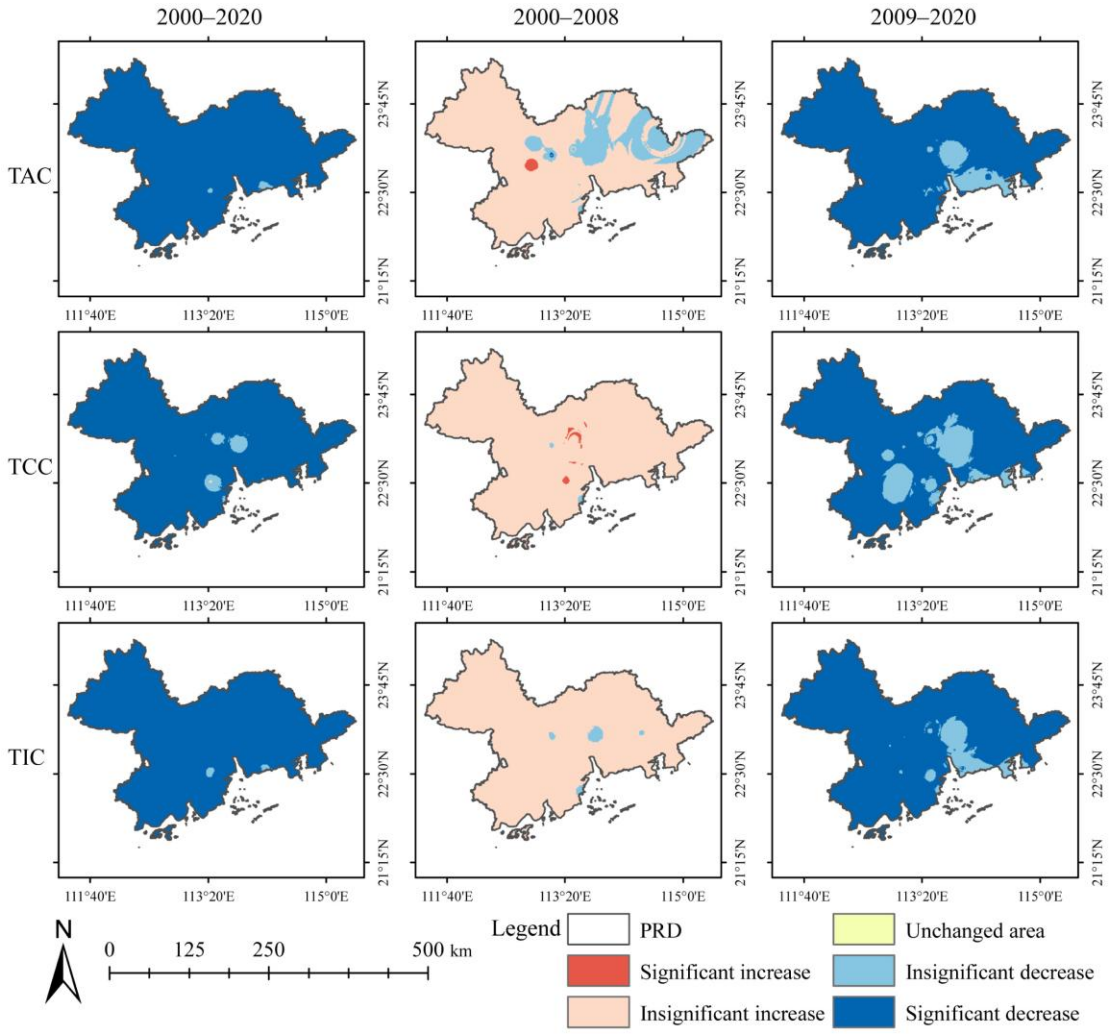


Figure S4. Spatial pattern and significance test (p<0.05) of total ion concentration in precipitation in the PRD from 2000 to 2020.

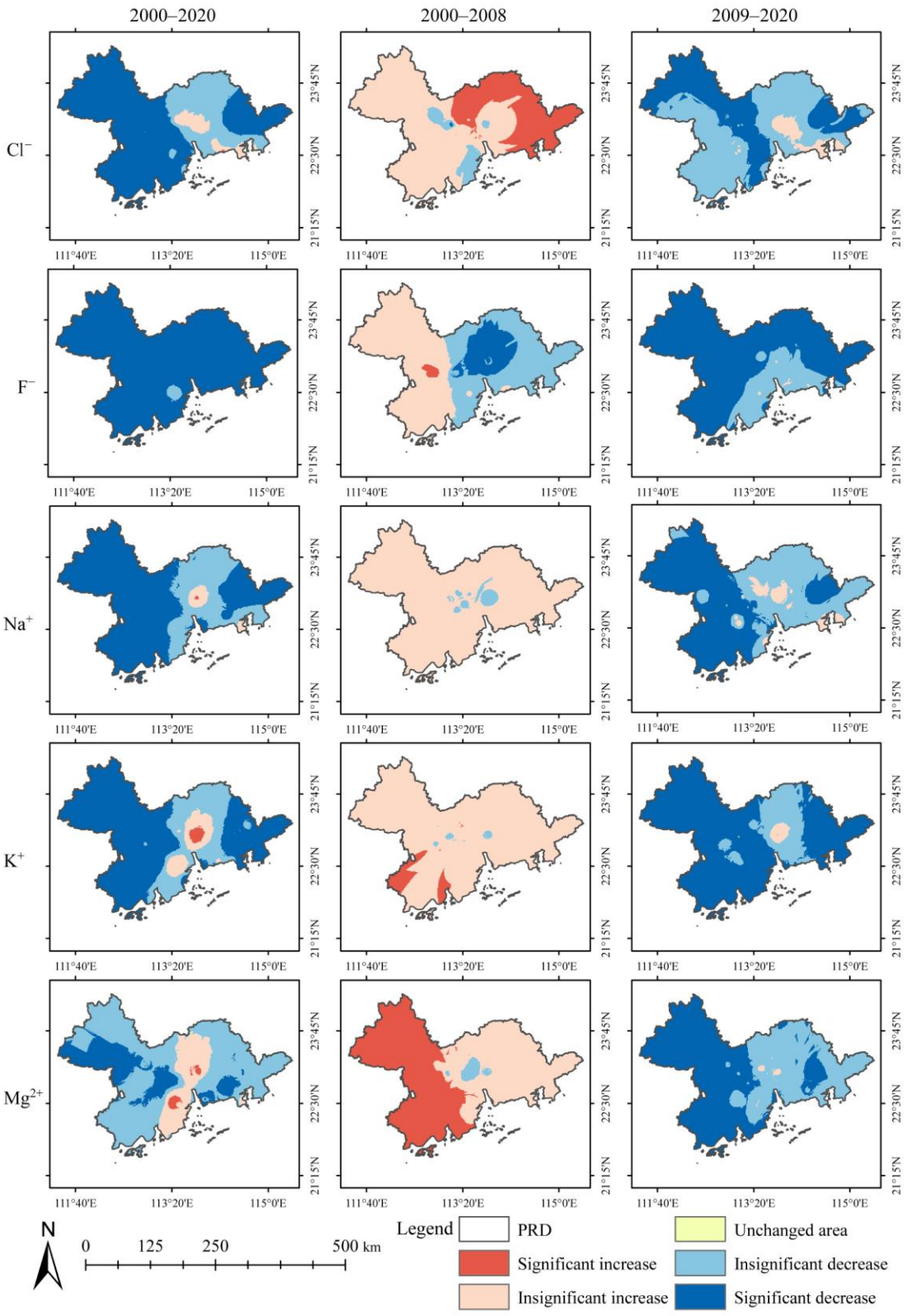


Figure S5. Spatial pattern and significance test (p<0.05) of minor ion concentration in precipitation in the PRD from 2000 to 2020.

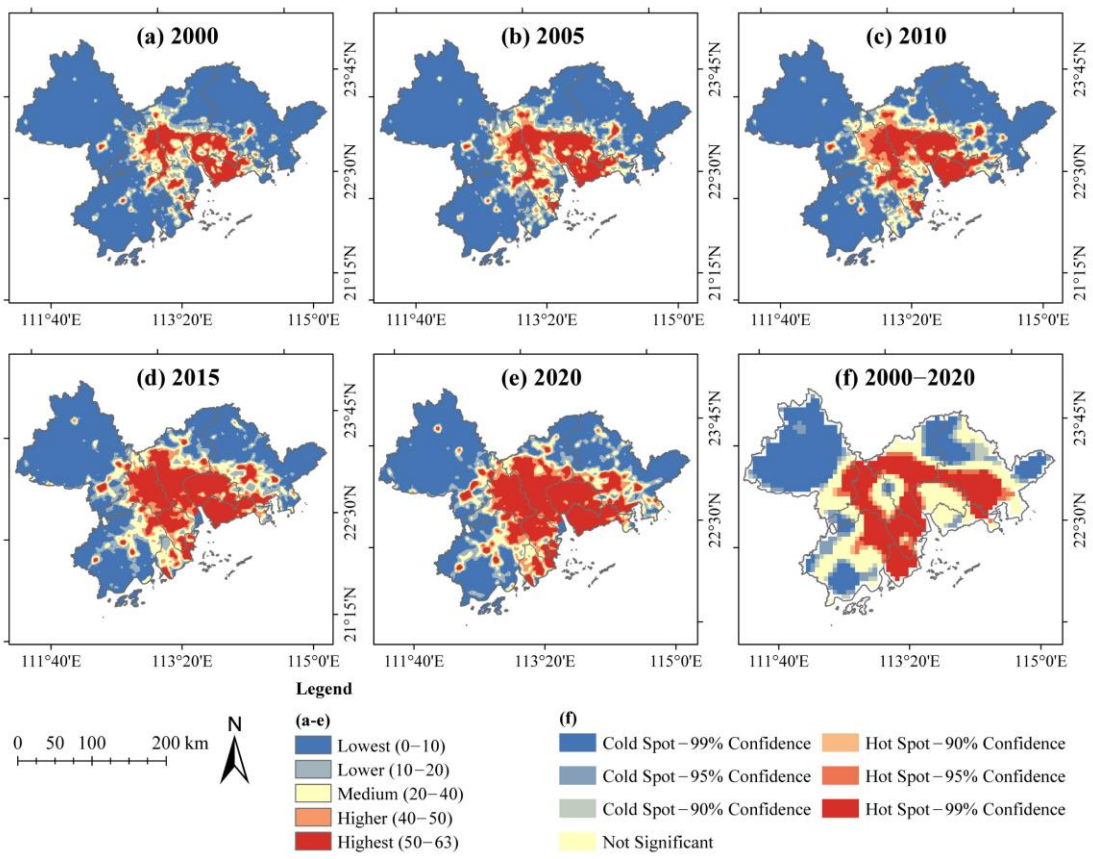


Figure S6. Spatial patterns (a–e) and changing hotspots of nighttime light (NTL) from 2000 to 2020.

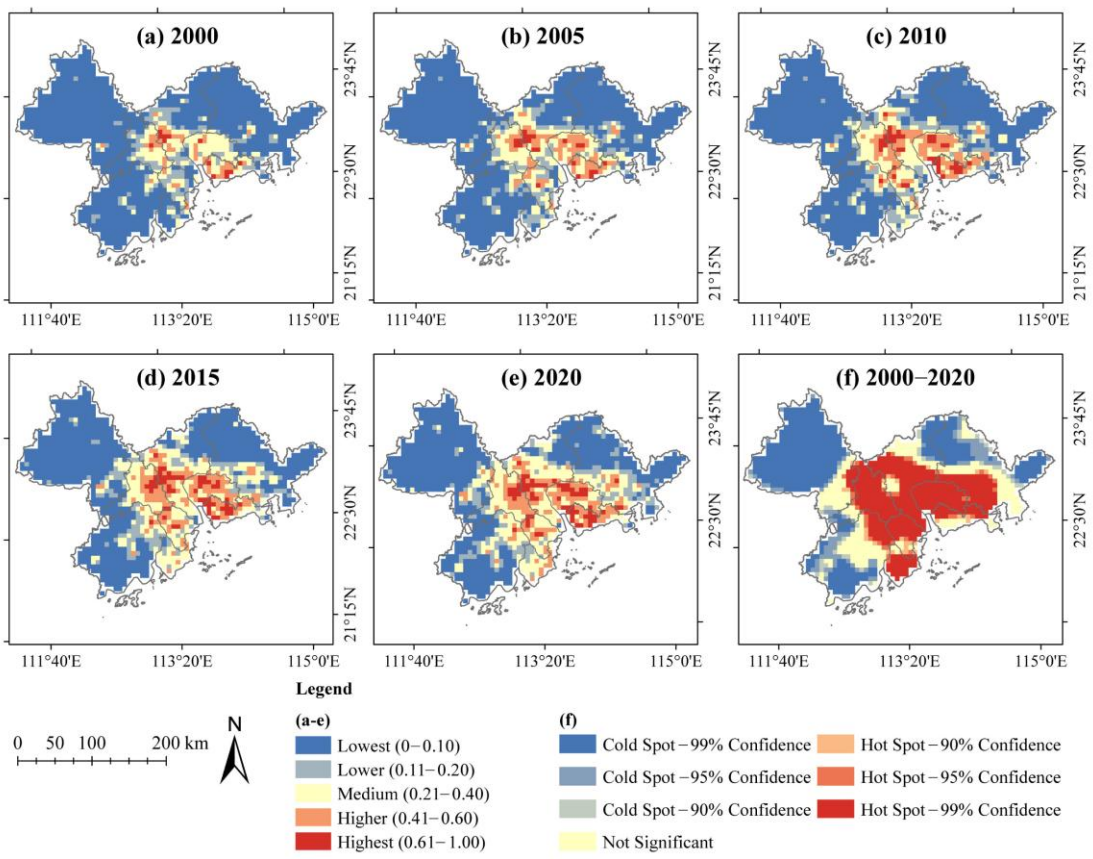


Figure S7. Spatial patterns (a–e) and changing hotspots of composite urbanization indicator (CUI) from 2000 to 2020.

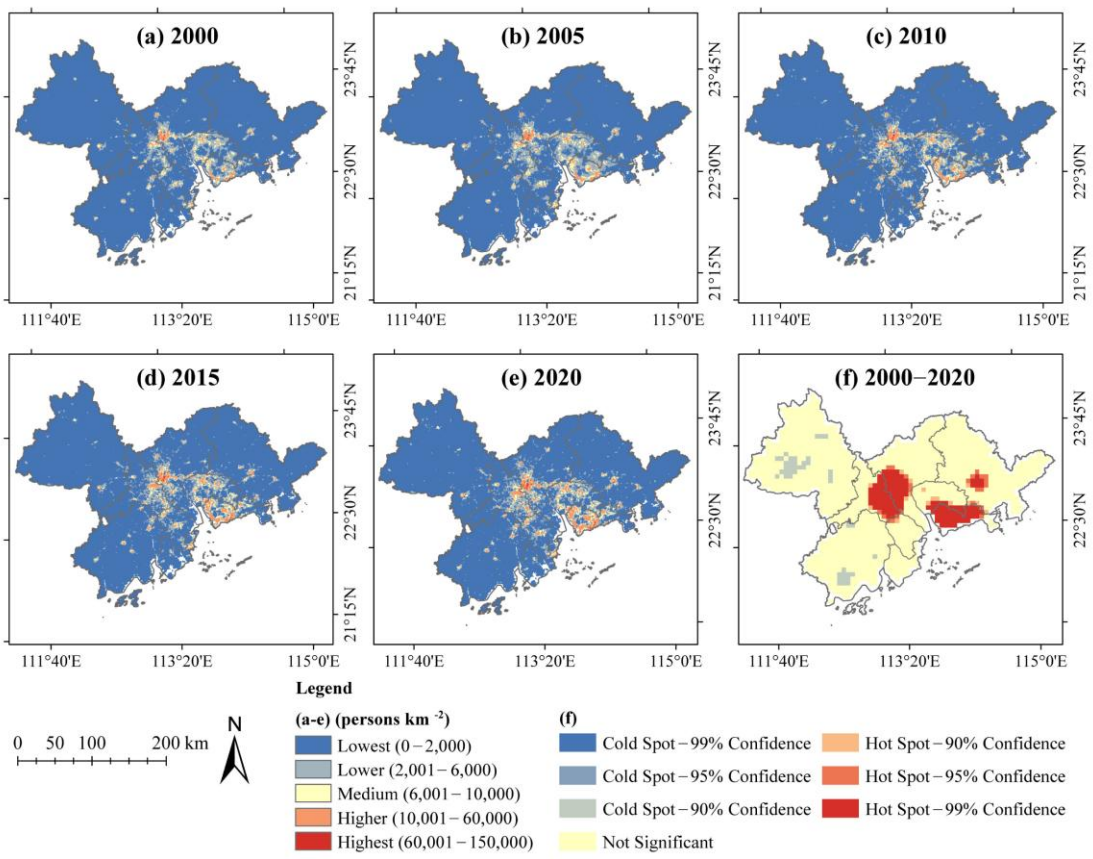


Figure S8. Spatial patterns (a–e) and changing hotspots of population density (POD, persons km^{-2}) from 2000 to 2020.

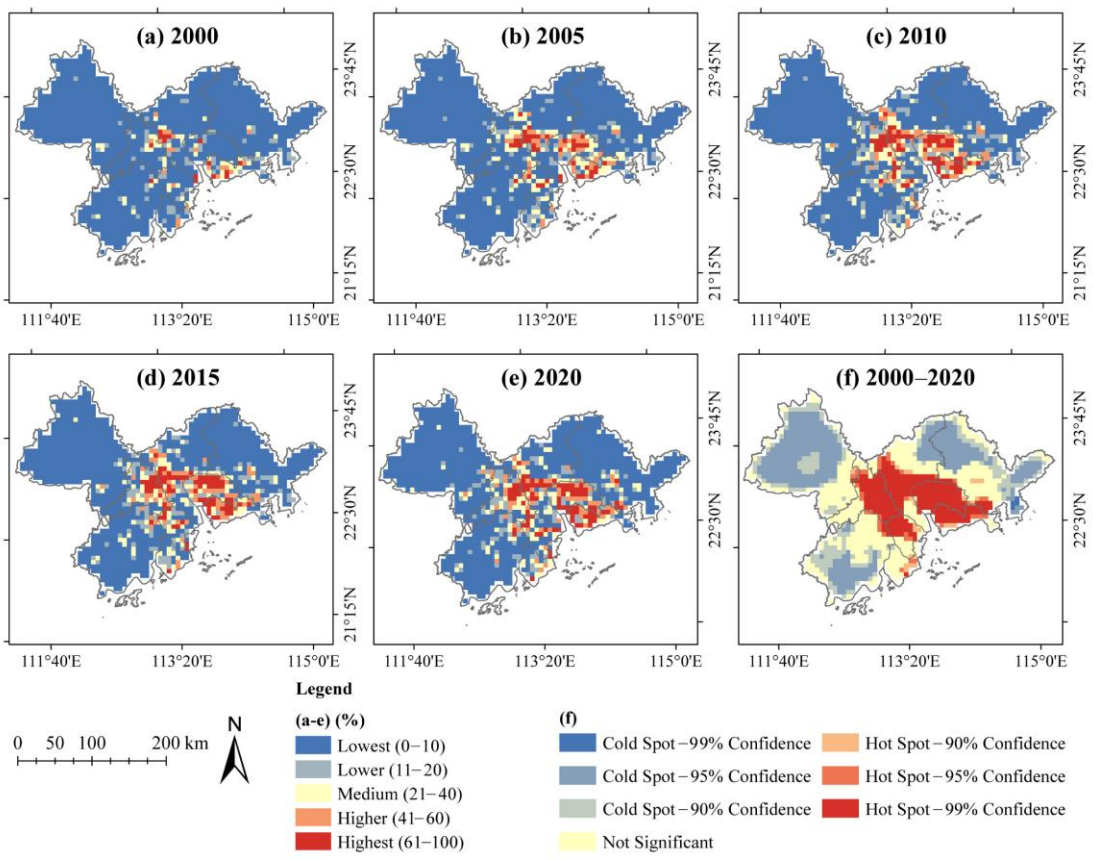


Figure S9. Spatial patterns (a–e) and changing hotspots of construction land proportion (CLP, %) from 2000 to 2020.

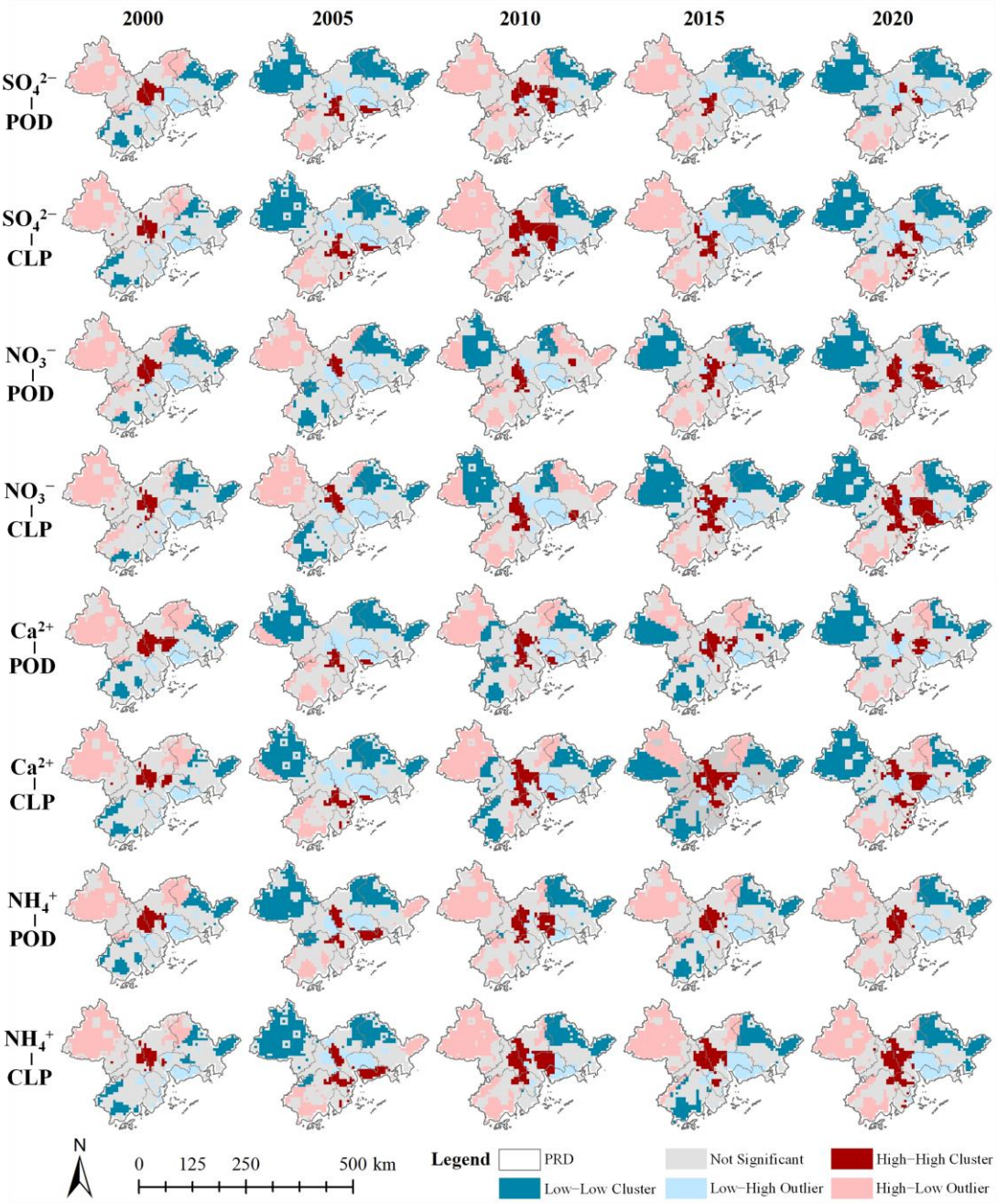


Figure S10. Bivariate LISA cluster map of precipitation ion concentration and population density (POD, persons km^{-2}) and construction land proportion (CLP, %) in the PRD area from 2000−2020.